

## Experimental study of Gamow-Teller transitions via the high-energy-resolution $^{18}\text{O}(^3\text{He}, t)^{18}\text{F}$ reaction: Identification of the low-energy “super” -Gamow-Teller state

H. Fujita<sup>1,\*</sup>, Y. Fujita<sup>1,2</sup>, Y. Utsuno<sup>3</sup>, K. Yoshida<sup>4</sup>, T. Adachi<sup>1</sup>, A. Algora<sup>5,6</sup>, M. Csatlós<sup>6</sup>, J. M. Deaven<sup>7,8,9</sup>, E. Estevez-Aguado<sup>5</sup>, C. J. Guess<sup>7,8,9,†</sup>, J. Gulyás<sup>6</sup>, K. Hatanaka<sup>1</sup>, K. Hirota<sup>1</sup>, R. Hutton<sup>7,8,9,‡</sup>, D. Ishikawa<sup>1</sup>, A. Krasznahorkay<sup>6</sup>, H. Matsubara<sup>1,§</sup>, F. Molina<sup>5,||</sup>, H. Okamura<sup>1,¶</sup>, H. J. Ong<sup>1</sup>, G. Perdikakis<sup>7,8,9</sup>, B. Rubio<sup>5</sup>, C. Scholl<sup>10,#</sup>, Y. Shimbara<sup>11,\*\*</sup>, G. Süsoy<sup>1,12</sup>, T. Suzuki<sup>1</sup>, A. Tamii<sup>1</sup>, J. H. Thies<sup>13</sup>, R. G. T. Zegers<sup>7,8,9</sup> and J. Zenihiro<sup>1,††</sup>

<sup>1</sup>Research Center for Nuclear Physics, Osaka University, Ibaraki, Osaka 567-0047, Japan

<sup>2</sup>Department of Physics, Osaka University, Toyonaka, Osaka 560-0043, Japan

<sup>3</sup>Advanced Science Research Center, Japan Atomic Energy Agency, Tokai, Ibaraki 319-1195, Japan

<sup>4</sup>Department of Physics, Kyoto University, Kyoto, 606-8502, Japan

<sup>5</sup>Instituto de Física Corpuscular, CSIC-Universidad de Valencia, E-46071 Valencia, Spain

<sup>6</sup>Institute of Nuclear Research (ATOMKI), H-4001 Debrecen, Post Office Box 51, Hungary

<sup>7</sup>National Superconducting Cyclotron Laboratory, Michigan State University, East Lansing, Michigan 48824-1321, USA

<sup>8</sup>Joint Institute for Nuclear Astrophysics, Michigan State University, East Lansing, Michigan 48824, USA

<sup>9</sup>Department of Physics and Astronomy, Michigan State University, East Lansing, Michigan 48824, USA

<sup>10</sup>Institut für Kernphysik, Universität zu Köln, 50937 Köln, Germany

<sup>11</sup>Graduate School of Science and Technology, Niigata University, Niigata 950-2181, Japan

<sup>12</sup>Department of Physics, Istanbul University, Istanbul 34134, Turkey

<sup>13</sup>Institut für Kernphysik, Westfälische Wilhelms-Universität, D-48149 Münster, Germany



(Received 26 July 2019; published 26 September 2019)

Using the high-resolution  $^{18}\text{O}(^3\text{He}, t)^{18}\text{F}$  reaction at  $0^\circ$  and at 140 MeV/nucleon, Gamow-Teller (GT) transitions were studied. A high energy resolution of 31 keV was achieved by applying dispersion matching techniques. The main part of the observed GT transition strength is concentrated in the transition to the  $^{18}\text{F}$  ground state (g.s.). The absolute values of the reduced GT transition strengths,  $B(\text{GT})$ , were derived up to  $E_x = 12$  MeV assuming proportionality between the  $B(\text{GT})$  values and the reaction cross sections at  $0^\circ$ . The  $B(\text{GT})$  value obtained from the  $\beta$  decay of  $^{18}\text{F}$  (g.s.)  $\rightarrow$   $^{18}\text{O}$  (g.s.) was used to determine the proportionality constant. A total  $B(\text{GT})$  of 4.06(5) was found and 76(1)% of the strength is concentrated to the ground state of  $^{18}\text{F}$ . The obtained  $B(\text{GT})$  values were compared with those from the  $^{18}\text{O}(p, n)^{18}\text{F}$  reaction and the mirror symmetric  $\beta^+$  decay of  $^{18}\text{Ne} \rightarrow ^{18}\text{F}$ . The candidates for  $1^+$  states with isospin  $T = 1$  were identified by comparison with the  $^{18}\text{O}(p, p')$  data. The results of shell-model and quasiparticle-random-phase approximation calculations suggest constructive contributions of various configurations to the  $^{18}\text{F}$  ground state, suggesting that this state is the low-energy super GT state.

DOI: [10.1103/PhysRevC.100.034618](https://doi.org/10.1103/PhysRevC.100.034618)

### I. INTRODUCTION

Gamow-Teller (GT) transitions with  $\Delta J^\pi = 1^+$  are mediated by the simple  $\sigma\tau$  operator and therefore are characterized by no orbital angular-momentum transfer ( $\Delta L = 0$ ) and spin-isospin flip nature ( $\Delta S = 1$  and  $\Delta T = 1$ ). Gamow-Teller transitions from a nucleus with  $Z$  and  $N$  to states in a neighboring nucleus with  $Z \mp 1$  and  $N \pm 1$  are called  $\text{GT}^\pm$  transitions by analogy from the  $\beta^\pm$  decay. Thus  $\text{GT}^\pm$  transitions have the nature of  $\Delta T_z = \pm 1$ , where  $T_z$  is the third component of isospin  $T$  and defined by  $(N - Z)/2$ .

\*hfujita@rcnp.osaka-u.ac.jp

<sup>†</sup>Present address: Department of Physics and Applied Physics, University of Massachusetts Lowell, Lowell, Massachusetts 01854, USA.

<sup>‡</sup>Present address: Institute for Defense Analyses, Alexandria VA USA, 22311.

<sup>§</sup>Present address: Tokyo Women's Medical University, Shinjuku, Tokyo, 162-8666, Japan.

<sup>||</sup>Present address: Comisión Chilena de Energía Nuclear, Post Office Box 188-D, Santiago, Chile.

<sup>¶</sup>Deceased.

<sup>#</sup>Present address: Institute for Work Design of North Rhine-Westphalia, Radiation Protection Services, 40225 Düsseldorf, Germany.

\*\*Present address: CYRIC, Tohoku University, Aramaki, Aoba, Sendai, 980-8578, Japan.

<sup>††</sup>Present address: RIKEN Nishina Center, Wako, Saitama 351-0198, Japan.

The reduced GT transition strength  $B(\text{GT})$  is an important physical quantity for our understanding of the nuclear structure [1–3] as well as for the calculation of astrophysical processes [4,5].

Absolute  $B(\text{GT})$  values can be determined directly from  $\beta$ -decay studies. However, these studies are limited by the decay  $Q$  values. On the other hand, charge exchange (CE) reactions, such as  $(p, n)$  or  $({}^3\text{He}, t)$ , performed at  $0^\circ$  and at intermediate incoming energies ( $E_{\text{in}} > 100$  MeV/nucleon), can be used to map the GT strengths over a wider range of excitation energies. For this purpose, one relies on the approximate proportionality between the reaction cross sections at  $0^\circ$  and the  $B(\text{GT})$  values [3,6,7].

The pioneering  $(p, n)$  reactions performed at 120–200 MeV revealed bumplike resonance structures of GT strength named Gamow-Teller resonance (GTR) in the high-excitation-energy ( $E_x$ ) region of 10–15 MeV. They have a width of a few MeV and carry the main part of the observed GT strength. Systematic study of GTRs have been reported for nuclei heavier than  $A \sim 50$  [2,8,9].

In the 1990s, the  $({}^3\text{He}, t)$  reaction at intermediate energy became available for the study of GT transitions. One-order-of-magnitude improvement in energy resolution has been achieved [3] in combining a magnetic spectrometer with dispersion matching techniques [10,11]. Due to the better resolution, the GTRs were resolved into many discrete excited states (GT states) in the  $({}^3\text{He}, t)$  reaction on  $f$ - and  $pf$ -shell target nuclei  ${}^{54}\text{Fe}$ ,  ${}^{58}\text{Ni}$ , and  ${}^{64}\text{Ni}$  [12–14]. In addition, in a recent systematic study on the  $f$ -shell  $N = Z + 2$  target nuclei  ${}^{42}\text{Ca}$ ,  ${}^{46}\text{Ti}$ ,  ${}^{50}\text{Cr}$ , and  ${}^{54}\text{Fe}$ , it was found that the distributions of GT strengths are strongly mass dependent [15,16]. In the  ${}^{54}\text{Fe}({}^3\text{He}, t){}^{54}\text{Co}$  reaction, the GT strength is mainly concentrated in the GTR region ( $E_x = 8$ –13 MeV). Moving on to the lighter nuclei  ${}^{50}\text{Cr}$  and  ${}^{46}\text{Ti}$ , less GT strength remained in the GTR region. Finally, in the  ${}^{42}\text{Ca}({}^3\text{He}, t){}^{42}\text{Sc}$  reaction, the GT strength was mostly concentrated in the  $1_1^+$  state, which was named the *low-energy super-GT* (LeSGT) state [15,16]. Note that the  ${}^{42}\text{Ca}$  nucleus has the  ${}^{40}\text{Ca} + 2n$  structure, where the  ${}^{40}\text{Ca}$  behaves as an LS-closed inert core for GT transition. The strong concentration of the GT strength is attributed to the contribution of the isoscalar-type attractive interaction that is active among the particle-particle-type configurations on the  ${}^{40}\text{Ca}$  inert core [16–18].

Since  ${}^{18}\text{O}$  nucleus also has the  ${}^{16}\text{O} + 2n$  structure, a similar concentration of the GT strength to the  $1_1^+$  state is expected in the  ${}^{18}\text{O} \rightarrow {}^{18}\text{F}$  transition. Using the  ${}^{18}\text{O}(p, n){}^{18}\text{F}$  CE reaction at  $E_p = 135$  MeV [19], at 118 MeV [20] and at 494 MeV [21], a strong concentration of the GT transition to the  ${}^{18}\text{F}$  ground state (g.s.) is reported. However, due to the energy resolution of 300–500 keV in the  $(p, n)$  reactions, details of the weak GT excitations could not be studied.

In this paper, we will present a study of GT transitions from  ${}^{18}\text{O}$  nucleus via the high-resolution  ${}^{18}\text{O}({}^3\text{He}, t){}^{18}\text{F}$  measurement performed at the Research Center for Nuclear Physics (RCNP), Osaka. Due to the high energy resolution realized by the use of the Grand Raiden magnetic spectrometer and application of the dispersion matching techniques [10,11], not only the strongly excited ground state but also weakly excited GT states could be studied up to 12 MeV.

## II. PROPERTIES OF SPIN-ISOSPIN EXCITATIONS

### A. Reduced transition strengths

The reduced GT transition strength  $B(\text{GT})$  is defined by

$$B(\text{GT}) = \frac{1}{2} \frac{1}{2J_i + 1} \frac{C_{\text{GT}}^2}{2T_f + 1} |M(\sigma\tau)|^2, \quad (1)$$

where  $C_{\text{GT}}$  and  $M(\sigma\tau)$  are the isospin Clebsch-Gordan (CG) coefficient and the doubly reduced  $\sigma\tau$  transition matrix element, respectively [3]. In CE reactions at  $0^\circ$  and at intermediate incident energies, the close proportionality between the reaction cross sections and the  $B(\text{GT})$  values is given by [3,6,7]

$$\frac{d\sigma_{\text{GT}}}{d\Omega} = \hat{\sigma}_{\text{GT}} f_{\text{GT}}(\omega) B(\text{GT}), \quad (2)$$

where  $\hat{\sigma}_{\text{GT}}$  is the GT unit cross section at energy transfer  $\omega = 0$ . The factor  $f_{\text{GT}}(\omega)$  gives the dependence of the GT cross section on the energy transfer and thus momentum transfer, which takes value 1 at  $\omega = 0$ .

In the Fermi transition, a similar proportionality

$$\frac{d\sigma_F}{d\Omega} = \hat{\sigma}_F f_F(\omega) B(F) \quad (3)$$

is expected.

The  $R^2$  value is defined as the ratio of GT and Fermi unit cross sections [7,22,23],

$$R^2 = \frac{\hat{\sigma}_{\text{GT}}}{\hat{\sigma}_F}, \quad (4)$$

which is a measure representing the ratio of strengths of the  $\tau$  and  $\sigma\tau$  terms of the effective interaction at a specific beam energy.

Proton inelastic scattering (IE) performed at small scattering angles, especially at  $0^\circ$  and intermediate energies, are also a good tool to study the  $\sigma\tau$  response of nuclei [3,24]. In analogy with the  $M1$  transitions via the electromagnetic interaction, we call  $\Delta J^\pi = 1^+$  transitions caused by the  $(p, p')$  reaction as  $M1_\sigma$  transitions [3].

Neglecting the contributions from the  $\sigma$  and other minor non- $\sigma\tau$  terms, a proportionality similar to Eq. (2) is expected in the  $(p, p')$  reaction [25–27],

$$\frac{d\sigma_{M1}}{d\Omega} \approx \hat{\sigma}_{M1} f_{M1}(\omega) B(M1_\sigma). \quad (5)$$

We define  $B(M1_\sigma)$  [3], the reduced transition strength assuming pure  $\sigma\tau$  interaction, as

$$B(M1_\sigma) = \frac{1}{2} \frac{1}{2J_i + 1} \frac{C_{M1}^2}{2T_f + 1} |M(\sigma\tau)|^2, \quad (6)$$

where  $C_{M1}$  is the isospin CG coefficient for the transitions to  $M1$  states. Assuming isospin symmetry and no contribution of meson exchange current (MEC) [28,29], identical  $M(\sigma\tau)$  values are expected for analogous transitions to GT and  $M1$  states.

### B. Isospin symmetry in $A = 18$ system

In Fig. 1, the  ${}^{18}\text{O} \rightarrow {}^{18}\text{F}$  GT transitions and the analogous transitions are summarized with the corresponding isospin CG coefficients. The  ${}^{18}\text{O}$  nucleus has  $T_z = (N - Z)/2 = +1$  and

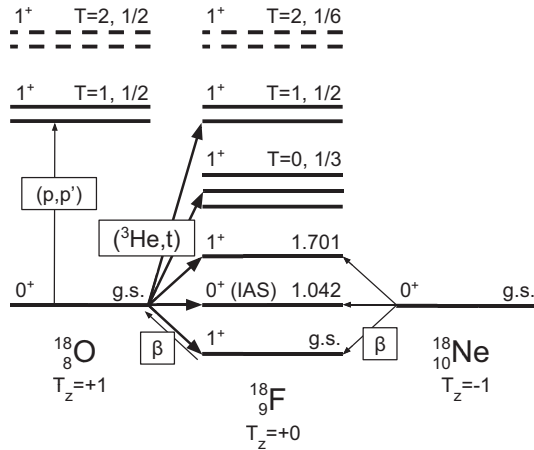


FIG. 1. Isospin structure of analogous GT and Fermi transitions among the  $A = 18$  isobars  $^{18}\text{O}$ ,  $^{18}\text{F}$ , and  $^{18}\text{Ne}$  with  $T_z = +1, 0, -1$ , respectively. The  $J^\pi$  values, isospin  $T$ , and the squared values of the isospin Clebsch-Gordan coefficients are given for the representative states.

initial isospin  $T_0 = 1$ . By the  $\text{GT}^-$  transitions from the  $^{18}\text{O}$  nucleus, therefore, GT states with  $T = 0, 1$ , and  $2$  in  $^{18}\text{F}$  ( $T_z = 0$ ) nucleus are nominally expected, as shown in Fig. 1. On the other hand, in the IE scattering such as  $(p, p')$ ,  $M1$  states with  $T = 1$  and  $2$  in  $^{18}\text{O}$  are expected. Because  $T_z = +1$  in  $^{18}\text{O}$ , a final isospin of  $T = 0$  is forbidden.

In the naive shell-model (SM) picture, the ground state of  $^{18}\text{O}$  is described by the LS-closed  $^{16}\text{O}$  inert core having  $T = 0$  plus two valence neutrons occupying the  $d_{5/2}$  orbit. This picture suggests that the final GT states in  $^{18}\text{F}$  have a proton ( $\pi$ ) and a neutron ( $\nu$ ) with configurations of  $(\pi d_{5/2}, \nu d_{5/2})$  and  $(\pi d_{3/2}, \nu d_{5/2})$  and the total isospin is determined by these two valence nucleons. Since  $T = 2$  cannot be formed by two nucleons, the GT states with  $T = 2$  cannot be excited in  $^{18}\text{F}$  without breaking the  $^{16}\text{O}$  inert core. For the same reason, the  $M1$  states with  $T = 2$  are not allowed in  $^{18}\text{O}$  nucleus. The  $T = 2$  states, therefore, are shown with dashed lines in Fig. 1.

Assuming isospin symmetry, the identical values are expected for the matrix elements  $M(\sigma\tau)$  in Eqs. (1) and (6) for the analogous GT and  $M1_\sigma$  transitions. Since the isospin CG coefficients  $C_{\text{GT}}$  and  $C_{M1}$  for the GT and  $M1_\sigma$  transitions to the  $T = 1$  states are the same (see Fig. 1), it is expected that the corresponding  $B(\text{GT})$  and  $B(M1_\sigma)$  values are also identical.

It should be noted that existence of large components of high-momentum neutrons in the  $^{16}\text{O}$  ground state due to the tensor interaction was suggested via the  $^{16}\text{O}(p, d)^{15}\text{O}$  reaction recently [30]. This result suggests that the inert  $^{16}\text{O}$  core is not closed and therefore the GT and  $M1$  states with  $T = 2$  can exist. However, even if they exist, the isobaric analog state (IAS) of  $^{18}\text{N}$  ground state having  $T = 2$  is expected at  $E_x \sim 16$  MeV in  $^{18}\text{O}$ , which corresponds to 17 MeV in  $^{18}\text{F}$ . This energy region is, however, out of observable region of the present data.

### III. EXPERIMENT

The  $^{18}\text{O}(^3\text{He}, t)^{18}\text{F}$  experiment was performed at the RCNP. The lateral and angular dispersion matching

techniques [10] were applied in order to realize high energy resolution and good scattering-angle resolution in the horizontal direction, respectively. A 140-MeV/nucleon  $^3\text{He}^{2+}$  beam of  $\sim 5$  enA from the RCNP ring cyclotron [31] was transported onto the target by using the WS course beamline [32]. A diagnostic method of dispersion matching and focusing conditions, the *faint beam method* [11], was applied in order to realize matching conditions.

The enriched  $^{18}\text{O}$  gas was filled in a gas cell target system [33] with aramid foil windows. For the background subtraction, the measurement with an aramid foil target was performed. Scattered tritons were momentum analyzed by the Grand Raiden magnetic spectrometer [34] located at  $0^\circ$ . The  $^3\text{He}^{2+}$  beam was stopped in a Faraday cup placed inside the first dipole magnet of Grand Raiden.

The tritons were detected by the two multiwire drift chambers (MWDCs) [35] placed along the focal plane with an angle of  $45^\circ$  relative to the central ray of the spectrometer. Each MWDC consists of two anode wire planes, with one set of sense wires stretched vertically (X) and another set of wires tilted at an angle of  $48.2^\circ$  (U) with respect to the vertical direction. By combining the X and U position information, vertical position (Y) in the focal plane was also obtained. Incident angles of the particles were obtained by the X and Y information from the two MWDCs. Two plastic scintillators downstream of the MWDCs were used for the particle identification and the generation of timing signals.

In order to achieve good scattering-angle resolution in the vertical direction, the over-focus mode [36] of Grand Raiden was applied. In combination with the angular dispersion matching technique [10], precise measurements of the scattering angles in both horizontal and vertical directions were realized. The precise  $0^\circ$  scattering angle was determined from the incident angle of singly charged  $^3\text{He}^+$  particles in the focal plane that are produced by atomic-electron capture processes in the target. Defocusing effects in the detector plane due to the kinematic recoil and aberration of the magnetic field were corrected by software.

## IV. DATA ANALYSIS

### A. Peak fitting and $E_x$ calibration

The  $^{18}\text{O}(^3\text{He}, t)^{18}\text{F}$  spectra with different vertical scales are given in Fig. 2, where the events within the scattering angles of  $0.0^\circ$ – $0.5^\circ$  are selected. As a result of the software corrections, an energy resolution of 31 keV ( $\Delta E/E = 7.4 \times 10^{-5}$ ) was achieved. The overview is given in Fig. 2(a), while the vertical scales are expanded by a factor of 8 and 100 in Figs. 2(b) and 2(c), respectively. Before the peak fitting analysis, the background (BG) events originated from the aramid foil windows of the gas cell and nitrogen in the contaminated air were subtracted. The spectrum after the BG subtraction is shown in Fig. 2(d).

Positions and counts of the peaks were obtained from the peak fitting analysis [37] using the peak shape of the strongest and isolated  $^{18}\text{F}$  ground state as a reference. The shapes of the states having decay widths  $\Gamma$  were reproduced by combining the reference peak shape and the width represented by a

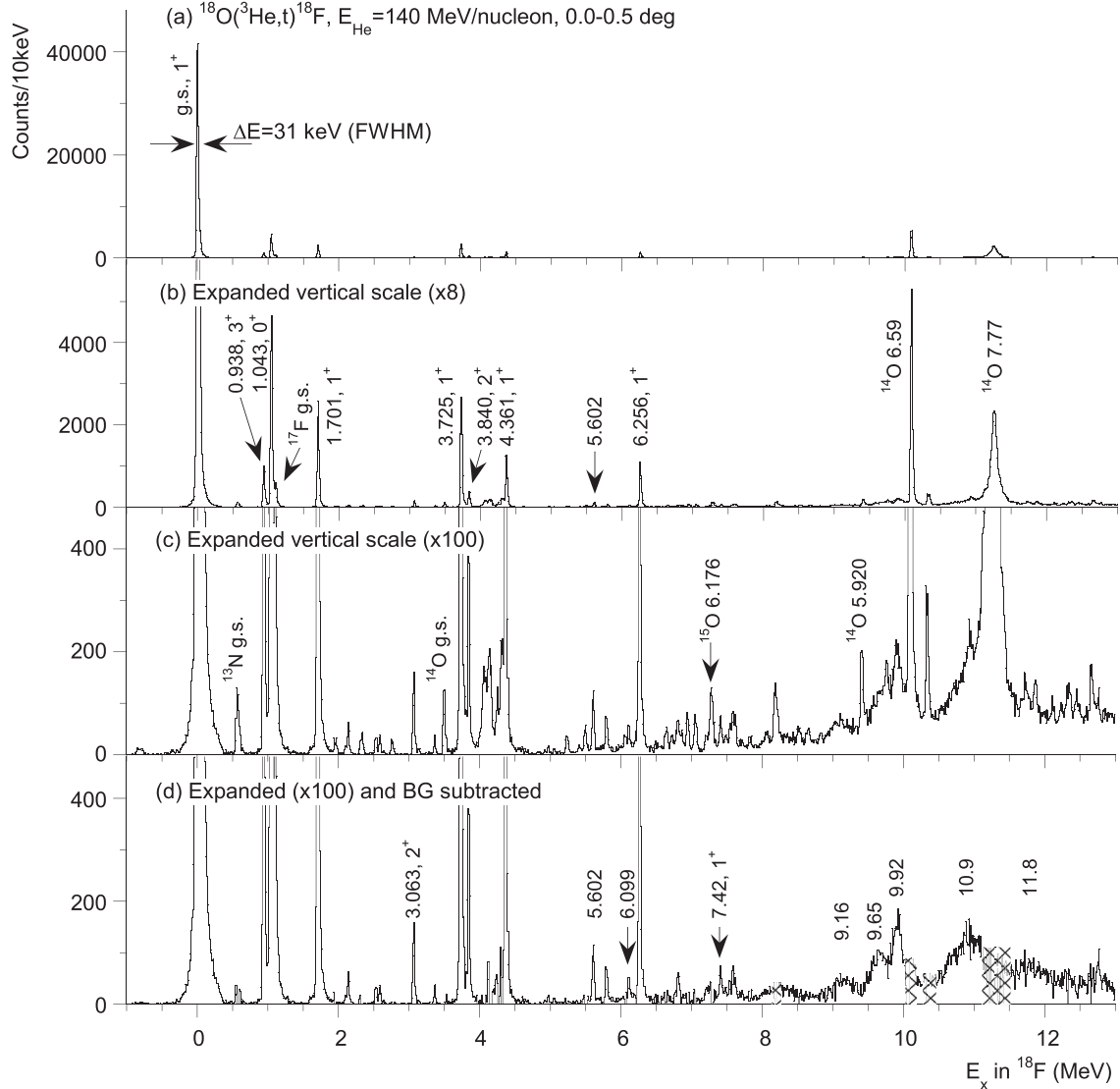


FIG. 2. Excitation energy spectra of  $^{18}\text{O}(^3\text{He}, t)^{18}\text{F}$  measurements for scattering angles  $0.0^\circ$ – $0.5^\circ$  (a) with full vertical scale, (b) with expanded scale ( $\times 8$ ), (c) with more expanded scale ( $\times 100$ ) before the BG subtraction, and (d) with the same scale as (c) but after the BG subtraction. An energy resolution of 31 keV is achieved. For details, see text.

Lorentzian function. Above the proton separation energy  $S_p$  of 5.6 MeV, a continuum caused by the quasifree scattering (QFS) [38] is expected. Amount of the QFS was estimated as a smoothly increasing function of excitation energy by connecting valleys of the spectra above the proton separation energy (see Fig. 4).

The relationship between the peak positions and the outgoing triton momenta were determined by the known states in  $^{12,13}\text{N}$  and  $^{16,18}\text{F}$  observed in the data using a polyethylene terephthalate ( $\text{C}_{10}\text{H}_8\text{O}_4$ ) film as a target. From the obtained relationship, the excitation energies of states in  $^{18}\text{F}$  were reconstructed. Due to the large difference between the  $Q$  values for  $^{18}\text{O}(^3\text{He}, t)^{18}\text{F}$  and  $^{12}\text{C}(^3\text{He}, t)^{12}\text{N}$  reactions ( $-1.67$  MeV and  $-17.36$  MeV, respectively), excitation energies of states in  $^{18}\text{F}$  can be determined by interpolation to 18 MeV.

In Table I, the  $E_x$  values obtained in the present analysis are compared with the evaluated values [39]. The recon-

structed excitation energies in  $^{18}\text{F}$  are in agreement with the evaluated values within 1 keV accuracies up to 5.6 MeV. Above this energy, the differences between the evaluated and reconstructed values are typically 5 keV. It should be noted that the uncertainties of the evaluated values are less than 0.3 keV below  $E_x = 5.6$  MeV, whereas above this excitation energy their uncertainties are about 1–3 keV.

### B. $\Delta L = 0$ identification

It is known that the angular distributions for the GT transitions, having the orbital angular-momentum transfer  $\Delta L = 0$  nature, show maximum cross section at  $0^\circ$  and a characteristic rapid decrease at larger scattering angles. On the other hand, such angular distribution is not expected for the  $\Delta L \geq 1$  transitions. In order to identify GT states, the angular distributions of the observed states were examined.

TABLE I. Evaluated  $E_x$  and  $J^\pi$  values of states up to 6.3 MeV and the  $E_x$  and  $Rr_4$  derived in the present analysis. For definition of the  $Rr_4$  ratio, see text.

Evaluated values <sup>a</sup>		Present analysis	
$E_x$ (MeV)	$J^\pi$	$E_x$ (MeV)	$Rr_4$
0.000	1 <sup>+</sup>	0.000	1.0 <sup>b</sup>
0.93720(6)	3 <sup>+</sup>	0.938	1.3
1.04155(8)	IAS, 0 <sup>+</sup>	1.043	1.2
1.70081(18)	1 <sup>+</sup>	1.701	1.1
3.06184(18)	2 <sup>+</sup>	3.063	1.9
3.72419(22)	1 <sup>+</sup>	3.725	1.3
3.83917(22)	2 <sup>+</sup>	3.840	1.5
4.36015(26)	1 <sup>+</sup>	4.361	1.0
5.60338(27)	1 <sup>+</sup> } 1 <sup>-</sup> }	5.602	1.9
5.60486(28)	1 <sup>-</sup> }		
5.786(2)	2 <sup>-</sup>	5.791	>10
6.0964(11)	4 <sup>-</sup> } (1 <sup>+</sup> ) }	6.099	>5
6.108(3)	(1 <sup>+</sup> ) }		
6.262(3)	1 <sup>+</sup>	6.256	1.1

<sup>a</sup>From Ref. [39].

<sup>b</sup> $Rr_4$  ratio of this state is normalized to be 1.

We define the ‘‘ratio of ratio’’ of counts,  $Rr$ , as follows. First, the counts of states in the spectra for the scattering angles of  $0.0^\circ$ – $0.5^\circ$ ,  $0.5^\circ$ – $0.8^\circ$ ,  $0.8^\circ$ – $1.2^\circ$ ,  $1.2^\circ$ – $1.6^\circ$ , and  $1.6^\circ$ – $2.0^\circ$ , which will be denoted with a subscript  $j = 0$ – $4$ ,

were normalized by the counts in the  $0.0^\circ$ – $0.5^\circ$  (i.e.,  $j = 0$ ) spectrum. These ratios for each state were further normalized by the corresponding ratios of the  $^{18}\text{F}$  ground state, which is the strongest GT state. Therefore, the  $Rr_j$  ratios are defined by

$$Rr_j = \frac{N_j}{N_0} \bigg/ \frac{N_j^{\text{g.s.}}}{N_0^{\text{g.s.}}}, \quad (7)$$

where  $N_j$  is the count for each state in the  $j$ th spectrum and  $N_j^{\text{g.s.}}$  is that for the ground state. All the states, therefore, take the ratio  $Rr_0 = 1$  by definition. For the states having the  $\Delta L = 0$  nature,  $Rr_{1-4} \sim 1$  are expected due to the similarity of angular distributions. On the other hand, for the states with  $\Delta L \geq 1$  nature,  $Rr_{1-4}$  values would be larger than unity because rapidly decreasing angular distribution is not expected. It should be noted that expected  $Rr$  value changes slightly as a function of  $E_x$  mainly due to the kinematic effect. By the distorted-wave Born approximation (DWBA) reaction calculation for the GT transition, difference of the  $Rr$  values at  $E_x = 0$  and 15 MeV is estimated to be less than 5%.

The obtained  $Rr_4$  ratios for the states below 6.5 MeV are summarized in Table I. In this region, the  $J^\pi$  values of most of the observed states are known and the 1<sup>+</sup> and 0<sup>+</sup> states show  $Rr_4 \sim 1$  as expected from their  $\Delta L = 0$  nature. On the other hand, the 2<sup>+</sup> states at 3.062 and 3.839 MeV and the 2<sup>-</sup> state at 5.786 MeV show larger  $Rr_4$  values as expected from their  $\Delta L \geq 1$  nature. It should be noted, however, that the 3<sup>+</sup> state at 0.937 MeV shows  $Rr_4$  value similar to those

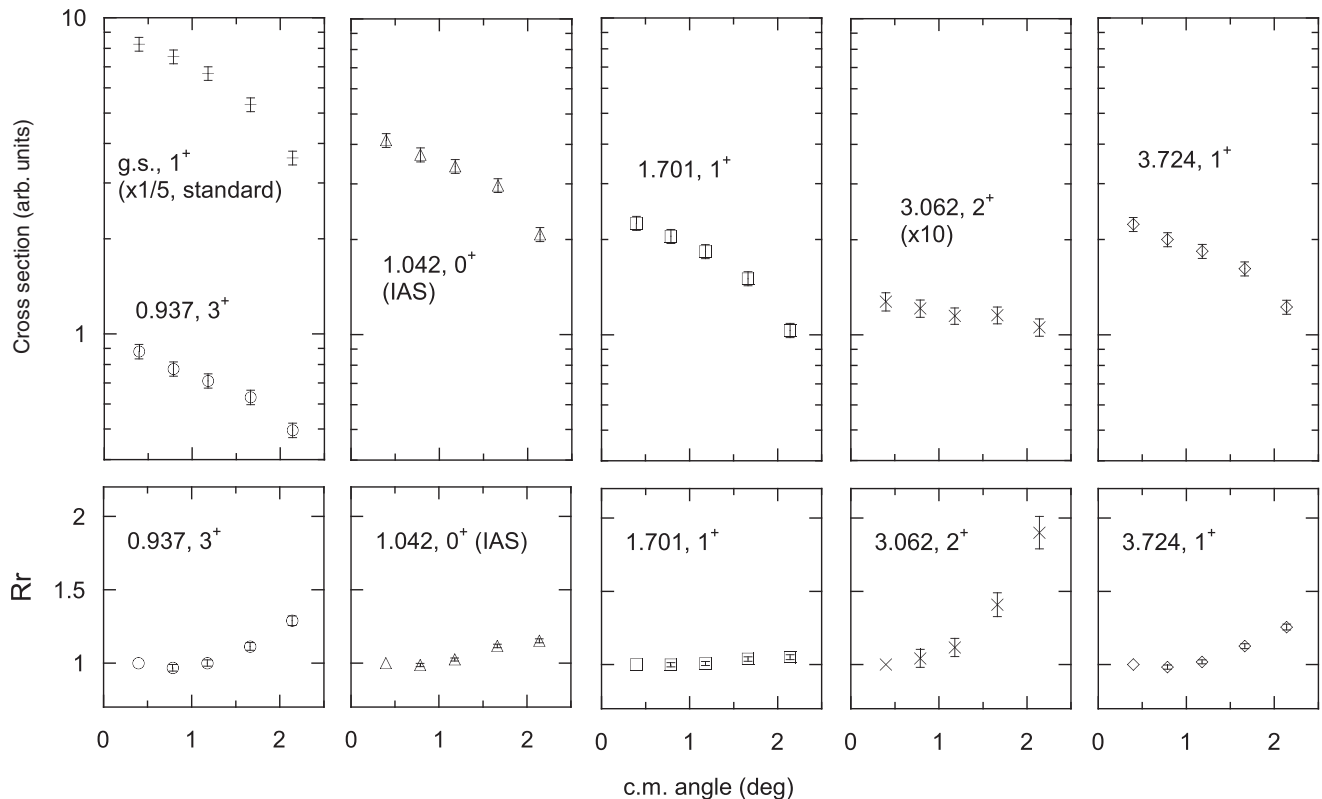


FIG. 3. Obtained angular distributions for the low lying states (top) and the corresponding  $Rr$  values (bottom). In the left-top panel, the angular distribution of the  $^{18}\text{F}$  ground state, which is used as the standard for the derivation of  $Rr$  ratios, is also shown. For details, see text.



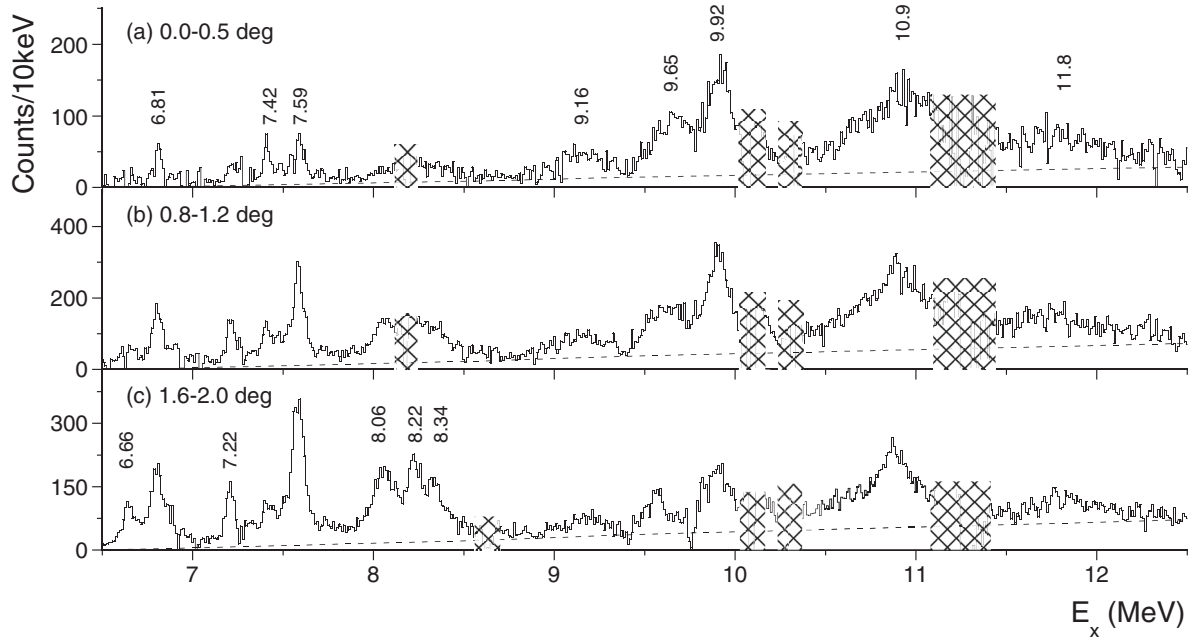


FIG. 4. The  $^{18}\text{O}(^3\text{He}, t)^{18}\text{F}$  spectra in the energy region of  $E_x = 6.5\text{--}12.5$  MeV for scattering angles (a)  $0.0^\circ\text{--}0.5^\circ$ , (b)  $0.8^\circ\text{--}1.2^\circ$ , and (c)  $1.6^\circ\text{--}2.0^\circ$ . Vertical axes are normalized by the corresponding solid angles. Events from contaminating nuclei are subtracted in all the spectra. The regions where the spectra are distorted by the background subtraction are hatched. The dashed lines show the QFS continuum assumed in the peak decomposition analysis. For details, see text.

of the  $1^+$  states, which was discussed in detail in Ref. [16]. As examples, angular distributions and the obtained  $Rr_{0-4}$  values for the low-lying states are shown in Fig. 3. The angular distribution of the  $^{18}\text{F}$  ground state, which was used as the normalization standard of the  $Rr_j$  values, is also shown.

For the weakly excited peak at 5.60 MeV,  $Rr_4 = 1.9$  was obtained. Since this peak can be a doublet of the  $1^+$  and  $1^-$  states at 5.603 and 5.605 MeV, respectively, the large  $Rr_4$  can be attributed to the contribution from the  $1^-$  state. The peak at 6.10 MeV, having  $Rr_4 > 5$ , can also be a mixture of the  $1^+$  and  $4^-$  states at 6.108 and 6.096 MeV. In both cases, even if the obtained counts in the  $0.0^\circ\text{--}0.5^\circ$  spectrum are purely from the  $1^+$  states, the estimated  $B(\text{GT})$  values for these peaks are less than our detection limit of  $B(\text{GT}) = 0.01$ .

In Figs. 4(a), 4(b), and 4(c), the  $^{18}\text{O}(^3\text{He}, t)$  spectra from 6.5 to 12.5 MeV are shown for the scattering angles  $0.0^\circ\text{--}0.5^\circ$ ,  $0.8^\circ\text{--}1.2^\circ$ , and  $1.6^\circ\text{--}2.0^\circ$ , where the events from the contaminating nuclei are subtracted. The deteriorated parts in the spectra due to the subtraction are hatched. The estimated QFS continuum is shown by dashed lines. Since the counts in Fig. 4 are normalized by the corresponding solid angles, relative peak heights of the states roughly represent the angular distributions.

In Table II,  $Rr_4$  ratios, excitation energies, and widths of peaks ( $\Gamma$ ) are summarized for the states above 6.5 MeV. Candidates for the corresponding states evaluated in Ref. [39] are also shown. Ambiguities of the width  $\Gamma$  was estimated from the results of the peak fitting analysis using the spectra for different scattering angles. For most of the states, more-or-less good agreements of widths were found.

A peak observed at 7.42 MeV becomes weaker at larger scattering angles, as can be seen in Figs. 4(a)–4(c). Although

this state shows relatively large  $Rr_4$  value of 2.3, we tentatively give  $\Delta L = 0$  assignment for this state since the  $Rr_{1-3}$

TABLE II. Evaluated  $E_x$  and  $J^\pi$  values, and natural decay width  $\Gamma$  for the states above 6.5 MeV and the  $E_x$ ,  $\Gamma$ ,  $Rr_4$ , and  $\Delta L$  values derived in the present analysis. For the definition of ratio  $Rr_4$ , see text.

Evaluated values <sup>a</sup>			Present analysis			
$E_x$ (MeV)	$J^\pi$	$\Gamma$ (keV)	$E_x$ (MeV)	$\Gamma$ (keV)	$Rr_4$	$\Delta L$
6.6437(8)	$2^-$	0.60(7)	6.66	30–50	>10	$\geq 1$
6.647(4)	$1^-$	91(4)				
6.803(2)	$1^+, 2, 3^+$	<2	6.81	80–90	>5	$\geq 1$
6.809(5)	$2^-$	88(2)				
7.201(2)	$(4^+)$	6.5	7.22	40–50	>5	$\geq 1$
7.247(2)	$(1^+)$	46.5				
7.406(2)	$1^+$	14.6(14)	7.42	20–30	2.3	(0) <sup>b</sup>
7.555(2)	$(1^-)$	30	7.59	70–80	>5	$\geq 1$
7.584(2)		9(2)				
8.064(6)	$\geq 4$	60	8.06	140–160	>10	$\geq 1$
8.209(2)	$2^-$	52	8.22	50–70	>10	$\geq 1$
8.238(2)	$4^+$	20				
			8.34	150–220	>5	$\geq 1$
			9.16	200–300	1.5	(0)
			9.65	170–230	0.75	(0)
			9.92	140–160	1.5	(0)
			10.9	400–600	1.5	(0)
			11.8	400–600	1.4	(0)

<sup>a</sup>From Ref. [39].

<sup>b</sup>See text.

TABLE III. The  $B(\text{GT})$  values obtained from the present  $^{18}\text{O}(^3\text{He}, t)^{18}\text{F}$  reaction, the  $^{18}\text{Ne}$   $\beta^+$  decay [39,47], the  $^{18}\text{O}(p, n)$  reactions [19–21], and the  $B(M1_\sigma)$  values from the  $^{18}\text{O}(p, p')$  reaction data [26]. The  $B(\text{GT})$  values from the  $(p, n)$  reactions [19–21] are renormalized using the present standard value from the  $^{18}\text{F}$   $\beta$ -decay data [39]. For the  $B(\text{GT})$  values from Ref. [19], additional ambiguities of 5% were added due to the relative ambiguity of the  $0^\circ$  cross sections. The units of the transition strengths from the  $(p, p')$  data [26] are converted to those of the  $B(M1_\sigma)$  values for the direct comparison. For details, see text.

Present data			$^{18}\text{Ne}$ $\beta$ decay			$(p, n)^a$			$(p, n)^b$		$(p, n)^c$		$(p, p')$	
$E_x$	$B(\text{GT}, \text{F})$	$T$	$B(\text{GT}, \text{F})$	$E_x$	$B(\text{GT})$	$T$	$E_x$	$B(\text{GT})$	$B(\text{GT})$	$E_x$ in $^{18}\text{O}$	$B(M1_\sigma)$			
g.s.	3.092(16)	0	3.123(24)	g.s.	3.092(16)	0	g.s.	3.092(16)	3.092(16)					
1.043 (IAS)	2	1	2.11(6)											
1.701	0.170(2)	0	0.131(5)	1.70	0.187(13)	0	1.70	0.21(2)						
3.725	0.173(2)	0		3.72	0.177(13)	0	3.72	0.19(2)						
4.361	0.090(2)	0		4.35	0.084(6)	0	4.35	0.09(1)						
5.602	<0.01	0												
6.099	<0.01	0												
6.256	0.069(1)	0		6.26	0.059(4)	0	6.11+6.26	0.08(1)						
7.42	<0.01	0												
9.16	0.03(1)	0												
9.65	0.05(1)	0		9.9	0.056(4)	(1)	9.9	0.14(2)		8.82	0.07(1)			
9.92	0.07(2)	1												
10.9	0.19(3)	1		10.9	0.084(6)	(1)	11.1	0.18(3)		10.10	0.31(4)			
11.8	0.07(2)	1		11.9	0.061(4)	(1)	12.0	0.12(2)						
Total	4.06(5)				3.80(3)			4.10(5)	4.2(5)	12.4–15.0				

<sup>a</sup>At  $E_p = 135$  MeV [19].

<sup>b</sup>At  $E_p = 118$  MeV [20].

<sup>c</sup>At  $E_p = 494$  MeV [21].

values of this state are within 1.0–1.5. It should be noted that there is a corresponding  $1^+$  state at 7.406 MeV [39]. Except for this state, all of the observed states between 6.5 and 8.5 MeV become stronger at larger scattering angles (see Fig. 4), suggesting their  $\Delta L \geq 1$  nature.

Above 9 MeV, most of the states show  $Rr_{1-3}$  of 0.9–1.3; however,  $Rr_4$  values are 1.4–1.5 except for the 9.65-MeV state with  $Rr_4 = 0.75$ . As shown in Figs. 2(c)–2(d) and Fig. 4, this region suffers from the large BG events and the QFS continuum, which may introduce large ambiguities to the  $Rr_{1-4}$  values. Therefore, we give tentative  $\Delta L = 0$  assignments for these states as summarized in Table II.

### C. Estimation of the $f_{\text{GT}}(\omega)$ term

The energy transfer  $\omega$  dependence of the  $f_{\text{GT}}(\omega)$  value in Eq. (2) was estimated from the reaction cross sections calculated by a series of DWBA codes, WSAW, FOLD, and DWHI [40]. Optical potential parameters for the  $^{18}\text{O} + ^3\text{He}$  channel were estimated by interpolating the values derived for  $^{16}\text{O}$  and  $^{28}\text{Si}$  [41–44]. For the outgoing  $^{18}\text{F}$  + triton channel, the well depths were multiplied by a factor of 0.85 without changing the geometrical parameters following the arguments given in Ref. [45]. In these calculations, pure  $\sigma\tau$ -type interaction was assumed.

The  $f_{\text{GT}}(\omega)$  estimation was performed as follows. First, averaged values of the cross sections at  $0^\circ$  assuming  $\pi d_{5/2} \rightarrow \nu d_{5/2}$  and  $\pi d_{5/2} \rightarrow \nu d_{3/2}$  transitions were calculated as a function of energy transfer  $\omega$ . The  $f_{\text{GT}}(\omega)$  values were then estimated by normalizing the averaged cross sections to 1

at  $\omega = 0$ . The estimated  $f_{\text{GT}}(\omega)$  value gradually decreases with increasing excitation energy and the amount of decrease from  $E_x = 0$  to 10 MeV was about 10%. Contributions of the  $\Delta L = 2$  component in the DWBA calculations at  $0^\circ$  was less than 0.1% in both configurations. For the Fermi transition, the  $f_F(\omega)$  term was estimated in a similar way.

### D. Derivation of the $B(\text{GT})$ values and the $R^2$ ratio

In order to derive the absolute  $B(\text{GT})$  values using Eq. (2), a standard  $B(\text{GT})$  value is needed. It was determined from the  $^{18}\text{F}$   $\beta^+$  decay, which connects the  $^{18}\text{F}$  g.s. ( $1^+$ ) and the  $^{18}\text{O}$  g.s. ( $0^+$ ) in opposite direction to the  $^{18}\text{O}(^3\text{He}, t)^{18}\text{F}$  reaction (see Fig. 1). From the half-life and the  $Q$  value given in Ref. [39], the  $B(\text{GT})$  value of 1.031(5) was obtained. Taking the factor of three for the reversed transition into account, a  $B(\text{GT})$  value of 3.092(16) was obtained for the  $^{18}\text{O}$  g.s.  $\rightarrow$   $^{18}\text{F}$  g.s. GT transition.

The derived  $B(\text{GT})$  values using this standard  $B(\text{GT})$  value are summarized in Table III. We estimate that reasonably precise  $B(\text{GT})$  values are deduced for the transitions with derived values larger than 0.01. Except for the  $^{18}\text{F}$  ground state, no strong GT transition was found. The total GT strength is 4.06(5) and 76(1)% of that concentrated in the transition to the ground state. Assuming no  $\text{GT}^+$  transition, it is 68% of the Ikeda GT sum rule value of  $3(N - Z) = 6$ .

The ratio of the GT and Fermi unit cross sections, i.e., the  $R^2$  value [7,22,23], was deduced from the present data. From the observed strengths of the  $^{18}\text{F}$  ground state and the IAS at 1.043 MeV in the  $0.0^\circ$ – $0.5^\circ$  spectrum,

TABLE IV. Deduced  $R^2$  values for  $^{18}\text{O}(^3\text{He}, t)^{18}\text{F}$  and  $^{42}\text{Ca}(^3\text{He}, t)^{42}\text{Sc}$  measurements and the related parameters.

	$^{18}\text{O}$		$^{42}\text{Ca}$		
	Counts ( $\times 10^4$ )	$B(\text{GT}, \text{F})$	$E_x$ (MeV)	Counts ( $\times 10^4$ )	$B(\text{GT}, \text{F})$
g.s. (GT)	16.32(4)	3.092(16)	g.s. (IAS)	3.45(5)	2
1.043 (IAS)	1.629(13)	2	0.611 (GT)	24.10(11)	2.17(5)
		$R^2 = 6.45(6)$			$R^2 = 6.45(18)$

$R^2 = 6.45(6)$  was obtained. For comparison, the  $R^2$  value from the  $^{42}\text{Ca}(^3\text{He}, t)^{42}\text{Sc}$  data [16] was also deduced from the  $1_1^+$  state at 0.611 MeV and the IAS (ground state). As a result, the identical  $R^2$  value with larger ambiguity of 6.45(18) was obtained. It should be noted that, from the GT and Fermi unit cross sections given in Ref. [46] as the functions of  $A$ , the  $R^2$  value of 4.94 and 6.99 are suggested for  $A = 18$  and 42, respectively. Numerical parameters are summarized in Table IV.

## V. DISCUSSION

### A. Comparison with the available data

In Table III, the present  $B(\text{GT})$  values derived from the present  $^{18}\text{O}(^3\text{He}, t)^{18}\text{F}$  data up to  $E_x = 12$  MeV are shown. The  $B(\text{GT})$  values from the  $^{18}\text{Ne}$   $\beta$  decay [39,47], the  $^{18}\text{O}(p, n)$  reactions [19–21], and the  $B(M1_\sigma)$  values from the  $^{18}\text{O}(p, p')$  scattering data [26] are also shown. In Fig. 5, these  $B(\text{GT})$  and  $B(M1_\sigma)$  values are shown together. The  $E_x$  value of the  $^{18}\text{O}(p, p')$  result is shifted by 1.1 MeV so that the analog states are expected to be aligned.

Between the  $B(\text{GT})$  values from the present study and those from the mirror symmetric  $^{18}\text{Ne} \rightarrow ^{18}\text{F}$   $\beta$  decay (see Fig. 1), isospin symmetry was examined. The  $B(\text{GT})$  and  $B(\text{F})$  values from the  $^{18}\text{Ne}$   $\beta$  decay were deduced by combining the recently published half-life [47] with the branching ratios and the decay  $Q$  value given in Ref. [39]. For the transition to the  $^{18}\text{F}$  ground state, the  $^{18}\text{Ne}$   $\beta$  decay gives a  $B(\text{GT})$  value of 3.123(24), which is consistent with the present standard value of 3.092(16) within the uncertainties. For the Fermi transition,  $B(\text{F})$  of 2.11(6) is also reasonably consistent with the expected value of  $N - Z = 2$ , suggesting consistency of the data. On the other hand, the  $B(\text{GT})$  value of 0.131(5) for the  $1_2^+$  state at 1.701 MeV is smaller than the present value of 0.170(2).

The  $B(\text{GT})$  values from the  $^{18}\text{O}(p, n)$  data at  $E_p = 135$  MeV [19], 118 MeV [20], and 494 MeV [21] in Table III are renormalized by using the present standard value of 3.092(16). Ambiguities of the  $B(\text{GT})$  values at 135 MeV were estimated from the relative uncertainties of the cross sections of 5% as given in Ref. [19]. For the  $1_2^+$  state at 1.701 MeV, the present value of 0.170(2) is 10–20% smaller than those from the  $(p, n)$  data at 135 MeV and at 118 MeV. For the states at 3.725, 4.361, and 6.256 MeV, consistent  $B(\text{GT})$  values within the uncertainties are found.

Above 9 MeV,  $E_x$  values for the GT states are reasonably consistent with the  $(p, n)$  measurements [19,20] as shown in Table III. Assuming the peaks at 9.65 MeV and 9.92 MeV are observed as one peak at 9.9 MeV in the  $(p, n)$  measurements,

the  $B(\text{GT})$  values from the present data and the  $E_p = 118$  MeV data [20] agree with each other. The  $B(\text{GT})$  value for the 11.1 MeV state from the  $E_p = 118$  MeV data is also consistent with the present data for the 10.9 MeV state.

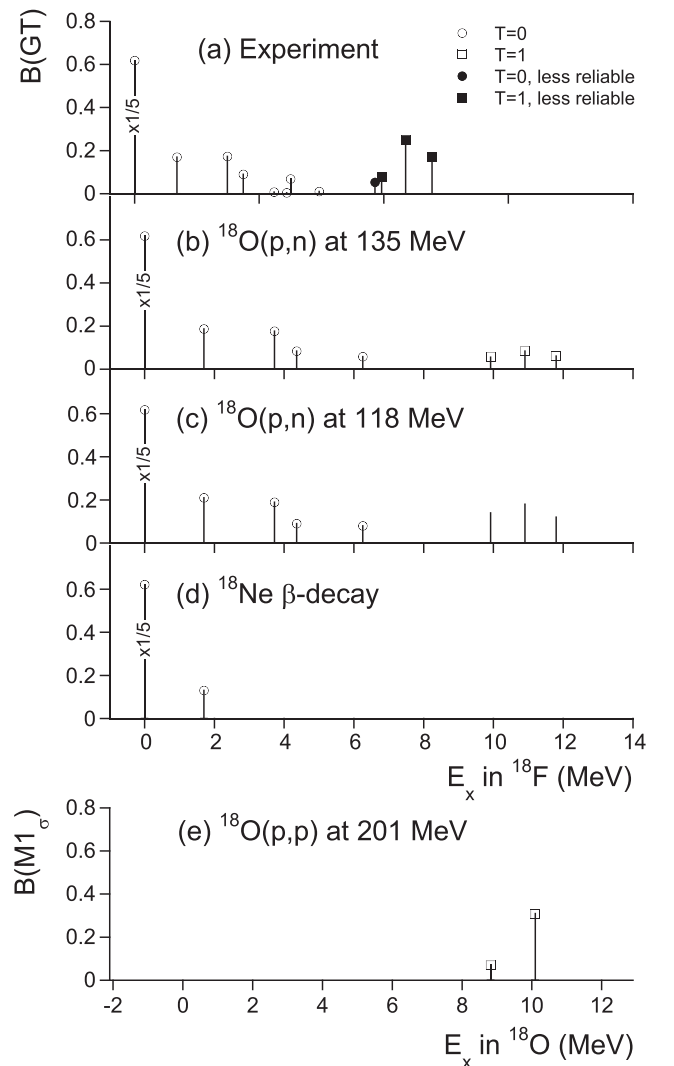


FIG. 5. The  $B(\text{GT})$  strength distributions from (a) the present  $(^3\text{He}, t)$  data, (b) the  $(p, n)$  data at 135 MeV [19], (c) the  $(p, n)$  data at 118 MeV [20], (d) the  $^{18}\text{Ne}$   $\beta$  decay [39,47], and (e) the  $B(M1_\sigma)$  values from the  $(p, p')$  data at 201 MeV [26]. The ground-state strengths are divided by a factor of 5. The horizontal axis of (e) is shifted by 1.1 MeV, so that the analog states are expected to be aligned.



As the total  $B(\text{GT})$  strengths, 3.80(3), 4.10(5), and 4.2(5) were obtained from the  $(p, n)$  data at  $E_p = 135$  MeV [19], 118 MeV [20], and 494 MeV [21], respectively. These values are consistent reasonably with the present value of 4.06(5).

As discussed above, it is expected that analogous  $1^+$  states with isospin  $T = 1$  are observed commonly in the present  $^{18}\text{O}(^3\text{He}, t)$  and  $^{18}\text{O}(p, p')$  data. From Eqs. (1) and (6) and isospin CG coefficients for the  $T = 1$  states (see Fig. 1),  $B(\text{GT})$  and  $B(M1_\sigma)$  are expected to be identical for analogous GT and  $M1$  states. The  $B(M1_\sigma)$  values shown in Table III were converted from the  $B(\sigma)$  values from the  $^{18}\text{O}(p, p')$  data [26] at 201 MeV, following the descriptions given in Refs. [3,28], neglecting contributions of non- $\sigma$   $\tau$ -type transitions.

For the state at 9.92 MeV,  $B(\text{GT})$  value of 0.07(2) was obtained from the present data. Since the IAS in  $^{18}\text{F}$  is at 1.043 MeV, the analog state is expected at around 8.9 MeV in  $^{18}\text{O}$ . At the corresponding energy of 8.82 MeV,  $1^+$  state with a consistent  $B(M1_\sigma)$  value of 0.07(1) was found from the  $^{18}\text{O}(p, p')$  data [26]. This fact suggests that these states are in analogous relationship and thus have isospin  $T = 1$ .

From the present data, the GT states were found at 10.9 and 11.8 MeV. As discussed above, the corresponding  $1^+$  states are also reported from the  $(p, n)$  data [19,20]. On the other hand, from the  $(p, p')$  data [26], a broad bump structure is reported at  $E_x = 10.10$  MeV with the  $B(M1_\sigma)$  value of 0.31(4). Since this value agrees with sum of the strengths for the states at 10.9 and 11.8 MeV, 0.26(8), within the ambiguities, we assign isospin  $T = 1$  for both of the 10.9 and 11.8 MeV states. The  $B(\text{GT})$  and  $B(M1_\sigma)$  values discussed here are summarized in Table III and Fig. 5.

In the  $(p, p')$  data [26], another bump structure was observed between 12.4 and 15 MeV. Since no corresponding strength is reported from the  $(p, n)$  data, this structure can be the giant dipole resonance, which is excited via the electromagnetic interaction.

### B. Low-energy super Gamow-Teller state

As is given in Table III, the  $B(\text{GT})$  value of 3.092(16) is obtained for the transition to the  $^{18}\text{F}$  g.s. ( $1_1^+$ ). This value corresponds to 76(1)% of the total strength up to 12 MeV. A similar concentration of the GT strength to the  $1_1^+$  state is reported in the  $^{42}\text{Ca}(^3\text{He}, t)^{42}\text{Sc}$  reaction [15,16]. A large  $B(\text{GT})$  value of 2.17(5), which corresponds to about 80% of the observed strength, was concentrated in the transition to the  $1_1^+$  state. Note that the  $A = 18$  and  $A = 42$  systems are expected to have the same structure in the sense that they consist of LS-closed core and two valence nucleons.

In the SM calculation using the GXPFIJ interaction for the GT transition from the  $^{42}\text{Ca}$   $0^+$  ground state to the  $^{42}\text{Sc}$   $1_1^+$  state, it was shown that several  $f$ - and  $p$ -shell configurations make an in-phase contributions [15,16]. Similarly, quasiparticle-random-phase approximation (QRPA) calculations also show that this state has a collective nature, which originates from the isoscalar attractive interaction among the particle-particle type configurations of the valence nucleons [15–17]. As a result, a large part of the available single-particle transition strengths are concentrated to the  $1_1^+$  GT

state in  $^{42}\text{Sc}$ . Because of the collective nature of this state, the  $1_1^+$  state at 0.611 MeV in  $^{42}\text{Sc}$  is the LeSGT state [15,16,18,48].

Let us discuss the properties of the  $^{18}\text{F}$  g.s. ( $1_1^+$ ) from an empirical view point. In Ref. [20], the GT strengths observed in the  $^{17}\text{O}(p, n)^{17}\text{F}$  reaction are presented. Starting from the  $^{17}\text{O}$  ground state with  $J^\pi = 5/2^+$ , two GT transitions to the  $^{17}\text{F}$  ground state ( $5/2_1^+$ ) and the state at 5.00 MeV ( $3/2_1^+$ ) with  $B(\text{GT}) = 1.062$  and 0.57 are reported. They would correspond to the  $\nu d_{5/2} \rightarrow \pi d_{5/2}$  and  $\nu d_{5/2} \rightarrow \pi d_{3/2}$  transitions on top of the inert  $^{16}\text{O}$  core, respectively. Here we notice that twice the sum of the  $B(\text{GT})$  values observed in the  $^{17}\text{O}(p, n)^{17}\text{F}$  reaction agrees well with the present  $B(\text{GT})$  value for the  $^{18}\text{F}$  ground state, i.e., 3.092(16). This fact suggests that the contributions of the  $\nu d_{5/2} \rightarrow \pi d_{5/2}$  and  $\nu d_{5/2} \rightarrow \pi d_{3/2}$  transitions make in-phase contributions in the transition to the  $^{18}\text{F}$  ground state and therefore this state has the nature of the LeSGT state.

This picture also suggests the existence of the state, in which the  $\nu d_{5/2} \rightarrow \pi d_{5/2}$  and  $\nu d_{5/2} \rightarrow \pi d_{3/2}$  contributions cancel each other. Such a state can be called an ‘‘anti-LeSGT’’ state [48]. In the SM calculation for the  $^{42}\text{Ca} \rightarrow ^{42}\text{Sc}$  case [16], strong cancellation between the  $\nu f_{7/2} \rightarrow \pi f_{7/2}$  and  $\nu f_{7/2} \rightarrow \pi f_{5/2}$  components was found in the transition to the  $1_2^+$  state, suggesting that this state has the nature of the anti-LeSGT state. We expect the anti-LeSGT state to exist also in  $^{18}\text{F}$ , with a similar destructive contribution between the  $\nu d_{5/2} \rightarrow \pi d_{5/2}$  and  $\nu d_{5/2} \rightarrow \pi d_{3/2}$  components.

### C. Shell-model calculations

The SM calculation for the GT transition of the  $^{42}\text{Ca} \rightarrow ^{42}\text{Sc}$  case showed that  $f$ - and  $p$ -shell configurations make an constructive contribution to the  $1_1^+$ , LeSGT state [15,16]. In order to study whether similar contributions exist also in the  $A = 18$  system or not, SM calculations were performed for the  $^{18}\text{O} \rightarrow ^{18}\text{F}$  case.

In Fig. 6, the  $B(\text{GT})$  strength distributions are shown from (a) the present  $^{18}\text{O}(^3\text{He}, t)$  data, those from the SM calculations using the interactions (b) the USDA [49] and (c) the USDB [49], and (d) the modified-PSDWBT [50]. The GT quenching factor is not included.

To 8 MeV, the observed fragmentation of the GT strength distribution [Fig. 6(a)] was well reproduced by the modified-PSDWBT calculation [Fig. 6(d)]. This would be because the modified-PSDWBT interaction can describe multiparticle multihole states within the  $p$ - $sd$  model space [50]. Above 8 MeV, higher level density was suggested by the calculation; however, the level density in this region cannot be derived from the present data because of the decay widths of the observed states (see Fig. 4).

Concentration of the GT strength to the  $1_1^+$  state was reproduced in all of the SM calculations. Our experiment shows that 74(1)% of the total strength is concentrated in the  $^{18}\text{F}$  g.s. ( $1_1^+$ ). On the other hand, in the SM calculations using the USDA, USDB, and modified-PSDWBT interactions, 86%, 87%, and 78% of the total strength, respectively, are concentrated in the  $1_1^+$  state.

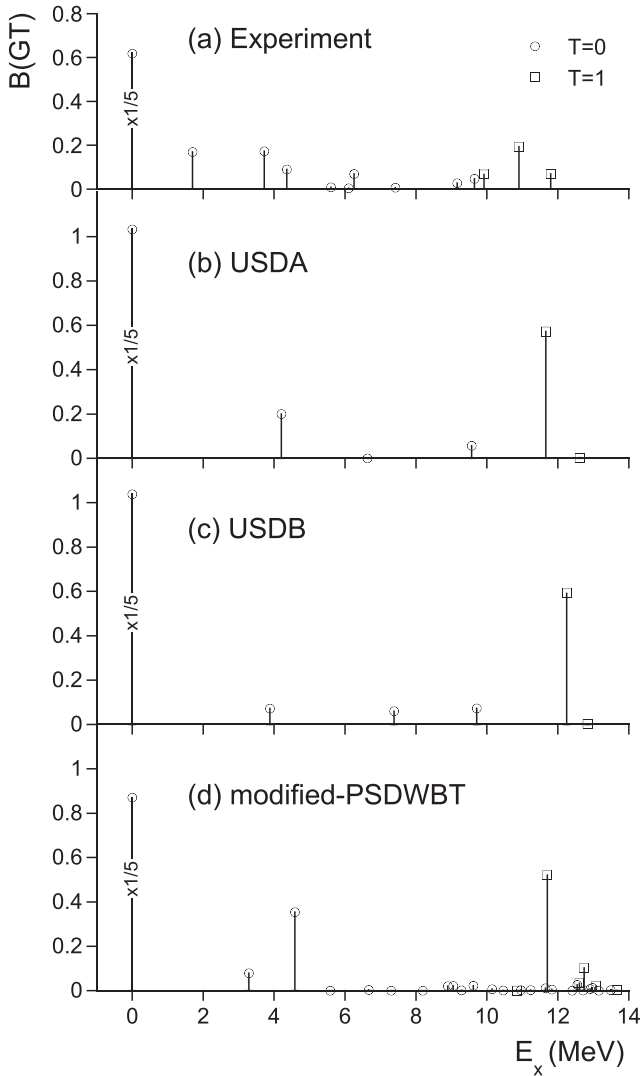


FIG. 6. The  $B(GT)$  strength distributions from (a) the present data and the shell-model calculations using the (b) USDA [49], (c) USDB [49], and (d) modified PSDWBT [50] interactions. The ground-state strengths are divided by a factor of 5.

In order to understand the transitions to the low-lying states, we examined the SM calculations in the simple  $sd$  model space using the USDA and USDB interactions. In Fig. 7, the GT matrix elements for different components from the calculations are illustrated for the  $1_1^+$ ,  $1_2^+$ , and  $1_3^+$  states. Square of the summed value of the GT matrix elements corresponds to the  $B(GT)$ . As expected from a naive SM picture, the components starting from the  $d_{5/2}$  orbit make large contributions and those from the  $d_{3/2}$  are small. Relatively large contributions are found from the  $2s_{1/2}$  orbit.

As can be seen in Fig. 7, in the transition to the  $1_1^+$  state, the constructive contributions from the  $\nu d_{5/2} \rightarrow \pi d_{5/2}$ ,  $\nu d_{5/2} \rightarrow \pi d_{3/2}$ , and  $\nu 2s_{1/2} \rightarrow \pi 2s_{1/2}$  components are realized. These results strongly support that this state has characteristics quite similar to the  $1_1^+$  state in  $^{42}\text{Sc}$  [15,16].

In the transition to the  $1_3^+$  state, both the USDA and USDB calculations show strong cancellation between the  $\nu d_{5/2} \rightarrow$

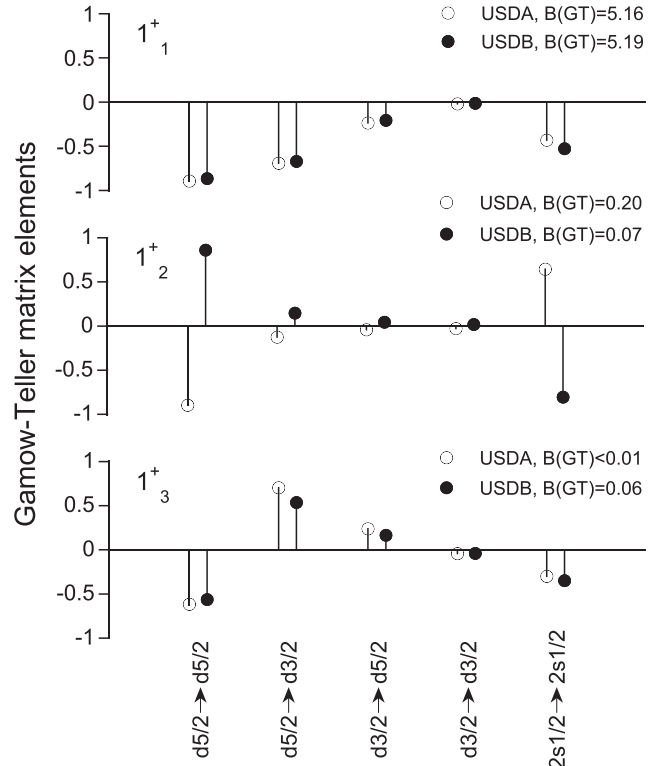


FIG. 7. The Gamow-Teller matrix elements for the three low-lying  $1^+$  states obtained by the USDA (open circle) and USDB (filled circle) interactions. The corresponding  $B(GT)$  values are shown together. For details, see text.

$\pi d_{5/2}$  and  $\nu d_{5/2} \rightarrow \pi d_{3/2}$  components, which makes  $B(GT)$  values small (see Fig. 7). Note that the absolute values of the GT matrix elements are similar to those in the  $1_1^+$  state. These results suggest that the  $1_3^+$  state have the characteristics of an anti-LeSGT state. The  $1_3^+$  state appears at 6.6 and 7.4 MeV in the USDA and USDB results, respectively. In the present data, a few weakly excited GT states were found in this region; however, empirical identification of the anti-LeSGT state is not clear.

As we see in Fig. 7, strong cancellation between the  $\nu d_{5/2} \rightarrow \pi d_{5/2}$  and  $\nu 2s_{1/2} \rightarrow \pi 2s_{1/2}$  components is found for the  $1_2^+$  state in both of the USDA and the USDB results. This characteristic cancellation may suggest that the  $1_2^+$  state also has anti-LeSGT nature, like the  $1_3^+$  state.

As shown in Figs. 6(b)–6(d), all the SM calculations show characteristic concentration of  $T = 1$  GT strength around  $E_x \sim 12$  MeV. However, as described above and shown in Fig. 6(a), we suggest that the  $T = 1$  GT strength is fragmented in the  $E_x = 10$ –12 MeV region.

#### D. QRPA calculation

For the  $^{42}\text{Ca} \rightarrow ^{42}\text{Sc}$  case, the strong concentration of the GT strength to the  $1_1^+$  state was explained by the competition of isoscalar (IS) and isovector (IV) pairing interactions [15–17]. Following the  $A = 42$  case, let us discuss here the GT strength distribution in the  $^{18}\text{O} \rightarrow ^{18}\text{F}$  case from the similar point of view. For this purpose, a self-consistent

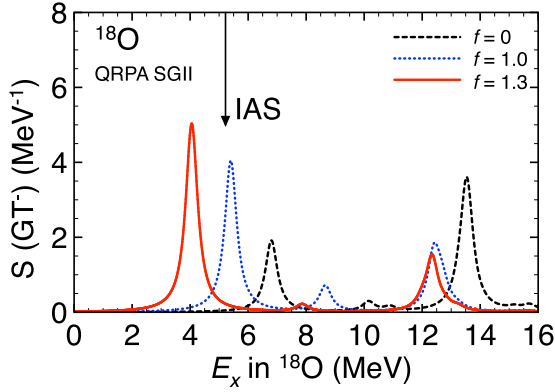


FIG. 8. Strength distributions of the  $^{18}\text{O} \rightarrow ^{18}\text{F}$  GT transitions obtained by the HFB + QRPA calculations employing the Skyrme SGII and the surface-type pairing interaction. The IS pairing interaction is included in the QRPA calculations with a factor  $f$ , a ratio of the strength for the IS pairing interaction to that for the IV pairing interaction. The arrow indicates the IAS obtained at  $E_x = 5.14$  MeV.

Hartree-Fock-Bogoliubov (HFB) plus QRPA calculation [51] using the Skyrme interaction SGII [52] was performed.

First, HFB and QRPA standard calculations including the IV,  $T = 1$ , pairing interaction were performed. Here the surface-type density-dependent contact interaction with a strength  $V_0 = -490$  MeV fm<sup>3</sup> was employed. Then we introduced the IS interaction between proton particle and neutron particle ( $\pi p$ - $\nu p$ ), i.e., the  $T = 0$  pairing interaction in the QRPA part of the calculation. Its strength is expressed by the factor  $f$  defined by the ratio of the strengths of the IS pairing interaction to that of the IV pairing interaction (for details, see Ref. [17]).

The obtained GT strength distribution varying the factor  $f$  is shown in Fig. 8, where the excitation energy  $E_x$  is given with respect to the ground state of the  $^{18}\text{O}$  nucleus. A width of 0.5 MeV was introduced to smear the strength distributions. We see that the GT strength is mainly divided into the lower-energy (LE) and higher-energy (HE) peaks. The origin of these states can be qualitatively explained by the involvement of the two-quasiparticle (2qp) configurations of  $\pi d_{5/2} \otimes \nu d_{5/2}$  and  $\pi d_{3/2} \otimes \nu d_{5/2}$ , which are formed by the  $\nu d_{5/2} \rightarrow \pi d_{5/2}$  and  $\nu d_{5/2} \rightarrow \pi d_{3/2}$  transitions, respectively. To make discussion comparable with the other part, components of the transitions will be described in the latter form.

As shown in Fig. 8, when  $f = 0$ , i.e., without the IS pairing interaction, the main part of the GT strength is in the HE peak

situated at 13.5 MeV. The LE peak at 6.8 MeV with smaller GT strength is mainly excited by a  $\nu d_{5/2} \rightarrow \pi d_{5/2}$  transition. With the increase in  $f$ , the peaks move to lower energy. At the same time, the GT strength of the HE peak becomes weaker and the LE peak acquires more strength (see Fig. 8). Eventually, in the case of  $f = 1.3$ , the LE peak appears 1 MeV below the IAS, being consistent with the  $E_x$  values of the  $1_1^+$  (ground state) and the IAS (1.043 MeV).

In Table V, the obtained  $B(\text{GT})$  values and the reduced GT matrix elements for different components with  $f = 1.3$  are summarized. The main contribution to the transition to the LE peak is the  $\nu d_{5/2} \rightarrow \pi d_{5/2}$  component. Furthermore, the  $\nu d_{5/2} \rightarrow \pi d_{3/2}$  and  $\nu d_{3/2} \rightarrow \pi d_{5/2}$  components make constructive contributions to the excitation of the LE peak. It should be noted that this result is reasonably consistent with the SM calculation. Thus, because of the strong collectivity suggested from both of the SM and QRPA calculations, we conclude that the  $1_1^+$  state in  $^{18}\text{F}$  is LeSGT state. The present QRPA calculation suggests that this collectivity is generated by the IS  $\pi p$ - $\nu p$  residual interaction.

With  $f = 1.3$ , we see a tiny peak at 7.9 MeV (see Fig. 8). As shown in Table V, the QRPA calculation also suggests that this state is generated by the destructive contribution mainly between the  $\nu d_{5/2} \rightarrow \pi d_{5/2}$  and the  $\nu d_{5/2} \rightarrow \pi d_{3/2}$  components, suggesting the existence of the anti-LeSGT state.

The HE peak is predominantly constructed by the remaining  $\nu d_{5/2} \rightarrow \pi d_{3/2}$  component that was not absorbed in the LE peak. Since this state locates  $\sim 7$  MeV higher than the IAS, the corresponding  $E_x$  value in  $^{18}\text{F}$  is about 8 MeV. This state may correspond to the excited states around 9–12 MeV [see Fig. 6(a)].

## VI. SUMMARY AND CONCLUSION

We have performed high-resolution  $^{18}\text{O}(^3\text{He}, t)^{18}\text{F}$  measurements at 140 MeV/nucleon and at an angle around  $0^\circ$ . Due to the high energy resolutions of 31 keV, most of the excited states in  $^{18}\text{F}$  are well separated. For the transition to the ground state of  $^{18}\text{F}$  ( $1_1^+$ ), a strong concentration of the Gamow-Teller transition strength was found. By using the standard  $B(\text{GT})$  value of 3.092(16) obtained from the  $\beta$  decay of  $^{18}\text{F}$ ,  $B(\text{GT})$  values for the observed  $1^+$  states were determined up to 12 MeV.

A total  $B(\text{GT})$  of 4.06(5) was found and 76(1)% of the strength is concentrated to the ground state. The obtained  $B(\text{GT})$  values were reasonably consistent with the available ( $p, n$ ), ( $p, p'$ ), and  $\beta$ -decay data.

TABLE V. Obtained  $B(\text{GT})$  values from the QRPA calculation applying a IS to IV strength ratio  $f = 1.3$  for the LE peak at  $E_x = 4.05$  MeV, the tiny peak at 7.86 MeV, and the HE peak at 12.4 MeV. The reduced matrix elements for each configuration are shown with the corresponding 2qp energy in MeV. Only those 2qp excitations possessing the RPA amplitude greater than 0.01 are shown. Note that the 2qp energies and  $E_x$  values are with respect to the  $^{18}\text{O}$  ground state. For details of calculation, see text.

$E_x$ in $^{18}\text{O}$ (MeV)	$\nu d_{5/2} \rightarrow \pi d_{5/2}$ 5.50	$\nu 2s_{1/2} \rightarrow \pi 2s_{1/2}$ 10.0	$\nu d_{3/2} \rightarrow \pi d_{5/2}$ 10.8	$\nu p_{1/2} \rightarrow \pi p_{1/2}$ 11.4	$\nu d_{5/2} \rightarrow \pi d_{3/2}$ 12.2	$B(\text{GT})$
4.05	0.754	0.063	0.103	-0.028	0.156	3.97
7.86	0.436	-0.138	-0.175	0.013	-0.291	0.16
12.4	-0.043	-0.043	-0.094		0.733	1.12

The SM calculations applying the USDA and USDB interactions suggest in-phase contribution of the  $\nu d_{5/2} \rightarrow \pi d_{5/2}$  and  $\nu d_{5/2} \rightarrow \pi d_{3/2}$  components in the GT transition to the  $^{18}\text{F}$  g.s. ( $1_1^+$ ) and thus the  $B(\text{GT})$  value becomes remarkably large. The mechanism causing the large  $B(\text{GT})$  value is similar to the one found for the  $1_1^+$  state in  $^{42}\text{Sc}$  [15,16].

The QRPA calculations were performed in order to investigate the roles of the effective IS pairing interaction in the GT transitions. The results of the calculations suggested the effective IS interaction causes the concentration of the GT strength to the  $1_1^+$  state. By increasing the strength of the IS interaction, the energy of the  $1_1^+$  state became lower and the GT strength was more concentrated. The constructive contribution of the two major configurations, i.e.,  $\nu d_{5/2} \rightarrow \pi d_{5/2}$  and  $\nu d_{5/2} \rightarrow \pi d_{3/2}$  is consistent with the SM calculations. Therefore we conclude that the  $1_1^+$  state in  $^{18}\text{F}$  is the LeSGT state.

The SM and QRPA calculations also suggested existence of the anti-LeSGT state, in which the GT strength is weak and the contributions of two major transitions cancel each other. In the present  $^{18}\text{O}(^3\text{He}, t)^{18}\text{F}$  data, a few candidates were found. However, it was not possible to identify the anti-LeSGT state specifically.

#### ACKNOWLEDGMENTS

The ( $^3\text{He}, t$ ) experiment was performed at RCNP, Osaka University, under Experimental Program No. E307. We thank

all the staffs of the accelerator group at RCNP for providing a high-quality beam. H.F. and Y.F. also acknowledge the support of MEXT, Japan, under Grants No. 18540270, No. 22540310, and No. 15K05104. Y.F. and B.R. are grateful for the support of the Japan-Spain collaboration program by JSPS and CSIC; A.A., E.E.A., and B.R. are thankful for the support of the Spanish Ministerio de Economía y Competitividad under Grants No. FPA2005-03993, No. FPA2008-06419-C02-01, No. FPA2011-24553, No. FPA2014-52823-C2-1-P, and No. FPA2017-83946-C2-1-P and the program Severo Ochoa (SEV-2014-0398). G.S. acknowledges the support of TUBITAK, Turkey under Research Scholarship No. BİDEB 2214. J.M.D., C.J.G., R.M., G.P., and R.G.T.Z. are grateful for the support of the U.S. NSF under Grants No. PHY-0606007 and No. PHY-0822648 (JINA). M.C., J.G., and A.K. acknowledge the support of the NKFI OTKA Foundation, Hungary, under Grant No. K124810. This work was in part supported by the RIKEN-CNS joint research project on large-scale nuclear-structure calculations. K.Y. acknowledges the support of the JSPS KAKENHI (Grants No. JP16K17687, No. JP18H04569, No. JP19K03824, and No. JP19K03872) and the JSPS-NSFC Bilateral Program for Joint Research Project on Nuclear mass and life for unraveling mysteries of the r-process. The QRPA calculations were performed on CRAY XC40 at the Yukawa Institute for Theoretical Physics, Kyoto University, and on COMA (PACS-IX) at the Center for Computational Sciences, University of Tsukuba.

- 
- [1] F. Osterfeld, *Rev. Mod. Phys.* **64**, 491 (1992); and references therein.
- [2] J. Rapaport and E. Sugarbaker, *Annu. Rev. Nucl. Part. Sci.* **44**, 109 (1994).
- [3] Y. Fujita, B. Rubio, and W. Gelletly, *Prog. Part. Nucl. Phys.* **66**, 549 (2011); and references therein.
- [4] G. M. Fuller, W. A. Fowler, and M. J. Newman, *Astrophys. J.* **252**, 715 (1982).
- [5] K. Langanke and G. Martínez-Pinedo, *Rev. Mod. Phys.* **75**, 819 (2003).
- [6] C. D. Goodman, C. A. Gouling, M. B. Greenfield, J. Rapaport, D. E. Bainum, C. C. Foster, W. G. Love, and F. Petrovich, *Phys. Rev. Lett.* **44**, 1755 (1980).
- [7] T. N. Taddeucci, C. A. Gouling, T. A. Carey, R. C. Byrd, C. D. Goodman, C. Gaarde, J. Larsen, D. J. Horen, J. Rapaport, and E. Sugarbaker, *Nucl. Phys. A* **469**, 125 (1987); and references therein.
- [8] M. N. Harakeh and A. van der Woude, *Giant Resonances*, Vol. 24 of Oxford Studies in Nuclear Physics (Oxford University Press, Oxford, 2001), and references therein.
- [9] C. Gaarde, *Nucl. Phys. A* **396**, 127c (1983).
- [10] Y. Fujita, K. Hatanaka, G. P. A. Berg, K. Hosono, N. Matsuoka, S. Morinobu, T. Noro, M. Sato, K. Tamura, and H. Ueno, *Nucl. Instrum. Methods B* **126**, 274 (1997).
- [11] H. Fujita, Y. Fujita, G. P. A. Berg, A. D. Bacher, C. C. Foster, K. Hara, K. Hatanaka, T. Kawabata, T. Noro, H. Sakaguchi, Y. Shimbara, T. Shinada, E. J. Stephenson, H. Ueno, and M. Yosoi, *Nucl. Instrum. Methods A* **484**, 17 (2002).
- [12] T. Adachi *et al.*, *Phys. Rev. C* **85**, 024308 (2012).
- [13] H. Fujita *et al.*, *Phys. Rev. C* **75**, 034310 (2007).
- [14] L. Popescu *et al.*, *Phys. Rev. C* **79**, 064312 (2009).
- [15] Y. Fujita *et al.*, *Phys. Rev. Lett.* **112**, 112502 (2014).
- [16] Y. Fujita *et al.*, *Phys. Rev. C* **91**, 064316 (2015).
- [17] C. L. Bai, H. Sagawa, G. Colò, Y. Fujita, H. Q. Zhang, X. Z. Zhang, and F. R. Xu, *Phys. Rev. C* **90**, 054335 (2014).
- [18] H. Sagawa, C. L. Bai, and G. Colò, *Phys. Scr.* **91**, 083011 (2016).
- [19] B. D. Anderson *et al.*, *Phys. Rev. C* **27**, 1387 (1983).
- [20] I. J. van Heerden *et al.*, *Phys. Rev. C* **59**, 1488 (1999).
- [21] D. J. Mercer *et al.*, *Phys. Rev. C* **49**, 3104 (1994).
- [22] Y. Fujita, *J. Phys.: Conf. Ser.* **20**, 107 (2005).
- [23] T. Adachi *et al.*, *Nucl. Phys. A* **788**, 70c (2007).
- [24] A. Tamii *et al.*, *Nucl. Instrum. Methods A* **605**, 326 (2009).
- [25] H. Matsubara *et al.*, *Phys. Rev. Lett.* **115**, 102501 (2015).
- [26] C. Djalali, G. M. Crawley, B. A. Brown, V. Rotberg, G. Caskey, A. Galonsky, N. Marty, M. Morlet, and A. Willis, *Phys. Rev. C* **35**, 1201 (1987).
- [27] G. M. Crawley, C. Djalali, N. Marty, M. Morlet, A. Willis, N. Anantaraman, B. A. Brown, and A. Galonsky, *Phys. Rev. C* **39**, 311 (1989).
- [28] Y. Fujita *et al.*, *Phys. Rev. C* **59**, 90 (1999).
- [29] Y. Fujita, B. A. Brown, H. Ejiri, K. Katori, S. Mizutori, and H. Ueno, *Phys. Rev. C* **62**, 044314 (2000).
- [30] H. J. Ong *et al.*, *Phys. Lett. B* **725**, 277 (2013).
- [31] I. Miura *et al.*, RCNP Annual Report 1991, Osaka University, p. 149.
- [32] T. Wakasa *et al.*, *Nucl. Instrum. Methods A* **482**, 79 (2002).
- [33] H. Matsubara *et al.*, *Nucl. Instrum. Methods A* **678**, 122 (2012).

- [34] M. Fujiwara *et al.*, *Nucl. Instrum. Methods A* **422**, 484 (1999).
- [35] T. Noro *et al.*, RCNP Annual Report 1991, Osaka University, p. 177.
- [36] H. Fujita, G. P. A. Berg, Y. Fujita, K. Hatanaka, T. Noro, E. J. Stephenson, C. C. Foster, H. Sakaguchi, M. Itoh, T. Taki, K. Tamura, and H. Ueno, *Nucl. Instrum. Methods A* **469**, 55 (2001).
- [37] H. Fujita *et al.*, RCNP Annual Report 2010, Osaka University, p. 3.
- [38] Y. Shimbara *et al.*, *Phys. Rev. C* **86**, 024312 (2012).
- [39] D. R. Tilley, H. R. Weller, C. M. Cheves, and R. Chasteler, *Nucl. Phys. A* **595**, 1 (1995); and references therein.
- [40] J. Cook and J. A. Carr, computer program FOLD/DWHI, Florida State University (unpublished), based on F. Petrovich and D. Stanley, *Nucl. Phys. A* **275**, 487 (1977); modified as described in J. Cook *et al.*, *Phys. Rev.* **30**, 1538 (1984); and R. G. T. Zegers, S. Fracasso, and G. Colò, (2006) (unpublished).
- [41] H. Fujita *et al.*, *Phys. Rev. C* **79**, 024314 (2009).
- [42] T. Yamagata, H. Utsunomiya, M. Tanaka, S. Nakayama, N. Koori, A. Tamii, Y. Fujita, K. Katori, M. Inoue, M. Fujiwara, and H. Ogata, *Nucl. Phys. A* **589**, 425 (1995).
- [43] J. Kamiya *et al.*, *Phys. Rev. C* **67**, 064612 (2003).
- [44] Y. Shimbara, R. G. T. Zegers, and H. Fujita (private communication, 2005).
- [45] S. van der Werf, S. Brandenburg, P. Grasdijk, W. A. Sterrenburg, M. Harakeh, M. Greenfield, B. A. Brown, and M. Fujiwara, *Nucl. Phys. A* **496**, 305 (1989).
- [46] R. G. T. Zegers *et al.*, *Phys. Rev. Lett.* **99**, 202501 (2007).
- [47] A. T. Laffoley *et al.*, *Phys. Rev. C* **92**, 025502 (2015).
- [48] Y. Fujita, Y. Utsuno, and H. Fujita, JPS Conf. Proc. **23**, 012030 (2018).
- [49] B. A. Brown and W. A. Richter, *Phys. Rev. C* **74**, 034315 (2006).
- [50] Y. Utsuno and S. Chiba, *Phys. Rev. C* **83**, 021301(R) (2011).
- [51] K. Yoshida, *Prog. Theor. Exp. Phys.* **2013**, 113D02 (2013).
- [52] N. V. Giai and H. Sagawa, *Phys. Lett. B* **106**, 379 (1981).